Integrative Modelling of Innate Immune Response Dynamics during Virus Infection

Ramya Boddepalli[a,c], Harsh Chhajer[a,b,c] and Rahul Roy[a,b]*

Author affiliations: [a] Department of Chemical Engineering, Indian Institute of Science, Bangalore 560012, India. [b] Department of Bioengineering, Indian Institute of Science, Bangalore 560012, India.

Orchid identifiers: RB: 0000-0002-0056-9980; HC: 0000-0001-9252-1855; RR: 0000-0003-3329-8803

[c] Equal contribution.

*Corresponding author: Rahul Roy. Department of Chemical Engineering, Indian Institute of Science, Bangalore, Karnataka, India- 560012. Phone: 91-80-2293-3115 Email: rahulroy@iisc.ac.in

Article classification: Biological Sciences | Microbiology and Immunology

Keywords: Positive-sense RNA virus | Innate immune signaling | Mathematical modeling | Interferon therapy | Virus-host dynamics

Abstract

Positive-sense RNA viruses that constitute a large class of human pathogens employ various strategies to evade host immune defences, complicating the development of effective antiviral therapies. Understanding the dynamic interaction between the viral life cycle and immune signaling is critical to designing effective antiviral strategies, yet the quantitative principles governing virus-host interactions remain poorly understood. In this study, we develop a mechanistic mathematical model that integrates the intracellular viral life cycle with key cellular innate immune pathways, including RIG-I–mediated sensing and JAK-STAT signaling. Our model reveals that virus-host interactions exhibit sharp bifurcation behaviour, where minor perturbations in immune strength or viral evasion capacity determine whether infections resolve or persist. Sensitivity analysis further revealed ISG mRNA translation and viral replication kinetics as dominant factors controlling infection outcomes, providing quantitative targets for therapeutic intervention. The model successfully recapitulates IFN desensitization phenomena and predicts optimal timing and dosing strategies for interferon-based prophylactic therapies. Together, our approach reveals fundamental principles that govern the delicate balance between viral persistence and immune control in RNA virus infections and potential avenues for future antiviral strategies.

Introduction

Positive-sense RNA viruses cause hundreds of millions of infections annually, including ∼770 million COVID-19 cases (7 million deaths) [1] reported since 2019, and ∼5–6 million dengue cases (∼20,000 deaths) [2] in 2023, with Hepatitis C alone responsible over 1.5 million new infections (∼290,000 deaths) per year [3, 4]. Once inside host cells, these viruses control the cellular machinery to translate their genomes, replicate, and produce new virions. This takeover also triggers host immune defences, igniting intricate interactions between viral elements, host components, and immune signaling pathways. The innate immune system, especially the interferon (IFN) response, acts as a vital front-line defence. However, (+) RNA viruses have evolved diverse tactics to dodge or suppress immune detection and response. Although experimental approaches have identified the main host and viral players and their roles in defining the extent of infection in cells, our ability to predict the outcome of such viral infection of the cell remains poor. Developing a deep and quantitative understanding of this cellular-level host-virus dynamics could be key to crafting effective antiviral strategies in the future.

The viral life cycle within the immune cell encompasses several coordinated, interconnected, and counteracting steps, including cellular entry, viral RNA translation, replication, assembly, and release of new virions. Conversely, some of the viral intermediates are detected by the innate immune surveillance system of cells, which activates mechanisms for viral clearance. For example, viral translation produces viral structural proteins required for viral assembly and viral non-structural proteins essential for cellular regulation and viral replication. Similarly, viral replication synthesizes the viral genome that fuels viral translation and is required for assembly. Viral replication occurs via a double-stranded RNA (dsRNA) intermediate, which can be detected by pattern recognition receptors (PRRs) such as RIG-I and MDA5. Upon detection, these receptors interact with the mitochondrial antiviral signaling protein (MAVS), initiating a signaling cascade that activates kinases including TBK1 and IKKϵ. These kinases phosphorylate transcription factors such as interferon regulatory factors (IRF3/7) and NF-κB, which translocate to the nucleus to induce the transcription of type I interferons (for example, IFN-α and IFN-β) [5, 6]. Secreted IFNs bind to their receptor (IFNAR) on the surface of the same or neighbouring cells, triggering the JAK-STAT pathway. Activated STAT1 and STAT2, together with IRF9, form the ISGF3 complex, which translocates to the nucleus to drive the expression of hundreds of interferon-stimulated genes (ISGs). These ISGs encode a diverse set of antiviral proteins that inhibit various stages of the viral life cycle, including entry, translation, replication, and assembly [7, 8]. Interferons are crucial signalling molecules in the immune system and are utilised therapeutically to enhance immune responses. However, prolonged or repeated exposure to IFN can lead to reduced cell responsiveness (IFN desensitisation), mainly due to slow recycling of related receptors.

On the other hand, (+)RNA viruses have evolved multiple immune evasion strategies to counteract the host defenses. These include direct cleavage or degradation of key signaling proteins such as MAVS,

TBK1, or STATs by viral proteases; interference with PRR activation or localization; inhibition of ISGF3 formation; and modulation of host gene expression to limit ISG output [9, 10, 11]. This creates complex feedback loops that result in the dichotomy of infection outcomes. Bifurcations in system behaviour underscore the delicate balance between viral replication and host defence mechanisms, revealing how small shifts in cellular conditions or virus–host interactions can lead to qualitatively different trajectories. This balance has been attributed to explain why individuals with marginally different immune responses often exhibit drastically different clinical outcomes [12, 13], even when infected with the same virus. Understanding these interactions is critical for predicting infection trajectories and identifying stages at which therapeutic interventions may be most effective [14, 15].

Many mathematical models have been developed that provide comprehensive insights into the viral life cycle processes [16, 17, 18, 19, 20] or the immune pathways [21, 22, 23, 24, 25]. For example, Dahari et al. predicted replicase binding bias, whereas more recent models have identified life cycle viral bottlenecks and been used to strategize antiviral treatments. Similarly, mathematical models of innate immune signaling have elucidated key features of JAK-STAT and RIG-I pathways modulating the IFN responses and recapitulated IFN-desensitization. However, these models either focus on the viral life cycle or the immune response, but not on their interactions.

Despite growing interest, relatively few studies mechanistically couple detailed viral replication with innate immune signalling [26, 27, 28, 29, 30]. Tan et al. [26] used delay differential equations to reveal immune–viral dynamics including bistability and oscillations. Rand et al. [27] combined agent-based and ODE models to simulate systemic innate responses but lacked molecular resolution. Zhang et al. [28, 29] modelled IFN signalling and captured bistability and feedback using minimal pathway detail. Castaño et al. [31] modeled antiviral targeting of viral RNAs, omitting broader immune signalling networks. These models offer valuable insights but often simplify molecular interactions. This limits the identification of host molecular targets to strategize antiviral plans.

Meanwhile, systems biology approaches and network models leverage high-throughput data to reconstruct protein–protein interaction (PPI) networks, gene regulatory circuits, and partial tissue topologies. These approaches have mapped thousands of regulatory interactions among interferon-stimulated genes (ISGs), PRRs, and downstream effectors, revealing key regulatory hubs and the broad architecture of innate immune signalling [32, 33, 34]. Network-based models, including those employing multiplex or spatial graph structures, have further elucidated how tissue topology and cytokine diffusion influence viral containment and immune response patterns [35]. However, these frameworks often treat viral replication or innate immune molecules as a static or external perturbation, rather than as a dynamic, evolving process subject to immune pressure and viral countermeasures. As a result, they may overlook how viral proteins actively disrupt specific nodes within the immune network, such as by cleaving PRR adaptors or targeting ISG proteins for degradation.

In this study, we present a mechanistic model that integrates detailed mathematical representations of the (+)RNA viral life cycle and host innate immune signalling pathways, along with their dynamic interactions. Since the cellular life cycle of (+)RNA viruses is highly conserved, we build our model upon the viral life cycle representation proposed by Chhajer et al. [19] - a model generic to (+)RNA viruses but detailed enough to generate molecular and mechanistic insights. Further, we adapt the comprehensive immune response model proposed by Burkart et al [36], which includes the RLR/IFN axis along with the popularly modeled pathways of JAK-STAT and RIG-I pathways, enabling a study into the inductor and effector functions of innate immune responses. Our integrated model recapitulates the observation of bifurcation in infection outcomes as well as the dose-dependent interferon desensitization. It also highlights the clustering of host factors that display similar temporal expression profiles and identifies receptors crucial for IFN desensitization. By perturbing this virus–immune crosstalk, the model reveals how infection outcomes are shaped by key factors such as the timing and magnitude of interferon (IFN) responses, the efficiency of virus-induced immune suppression, and the kinetics of viral translation, viral replication, and host ISG expression. We further evaluate the prophylactic potential of IFN and demonstrate how co-targeting viral replication or immune suppression mechanisms can enhance its efficacy. Overall, this work underscores the value of quantitative, systems-level modeling in dissecting virus–host dynamics. Our framework offers predictive insights for antiviral strategy design and advances the field of computational immunovirology, with broad relevance to (+)RNA virus infections.

Results

A cellular model of host-virus interactions

We developed our integrated model building on two existing ODE-based mathematical models. (a) Chhajer et al. [19] modeled the cellular life cycle of (+)RNA viruses, monitoring important viral molecules like viral RNA, proteins, and viral particles. (b) Burkart et al. [36] modeled the immune signaling network of RIG-I, MAVS and IFN pathways, at the cellular level accounting for molecular details. We introduced a few variables to integrate the two models (details in Methods and SI text) and a couple of parameters to account for the antiviral action of the immune system on the viral life cycle ($I_{V,N}$) and the virus-induced suppression of the immune response ($V_{I,N}$). We also account for the negative auto-regulation of the immune pathway (II, N), that is induced by certain interferon-stimulating genes (ISGs).

We simulated the model with parameter values estimated for Hepatitis C Virus (HCV) infection [19] and examined how these interactions affect the system dynamics. As the infection starts and immune pathways are triggered, one can look at various scenarios depending on the presence of cross-talks: (a) S_0, where subsequent virus-host interactions are ignored ($I_{V,N} = V_{I,N} = I_{I,N} = 0$), (b) S_a, where the immune response suppresses the viral life cycle but not itself ($I_{V,N} = 1; V_{I,} = I_{I,N} = 0$); (c) S_b, where

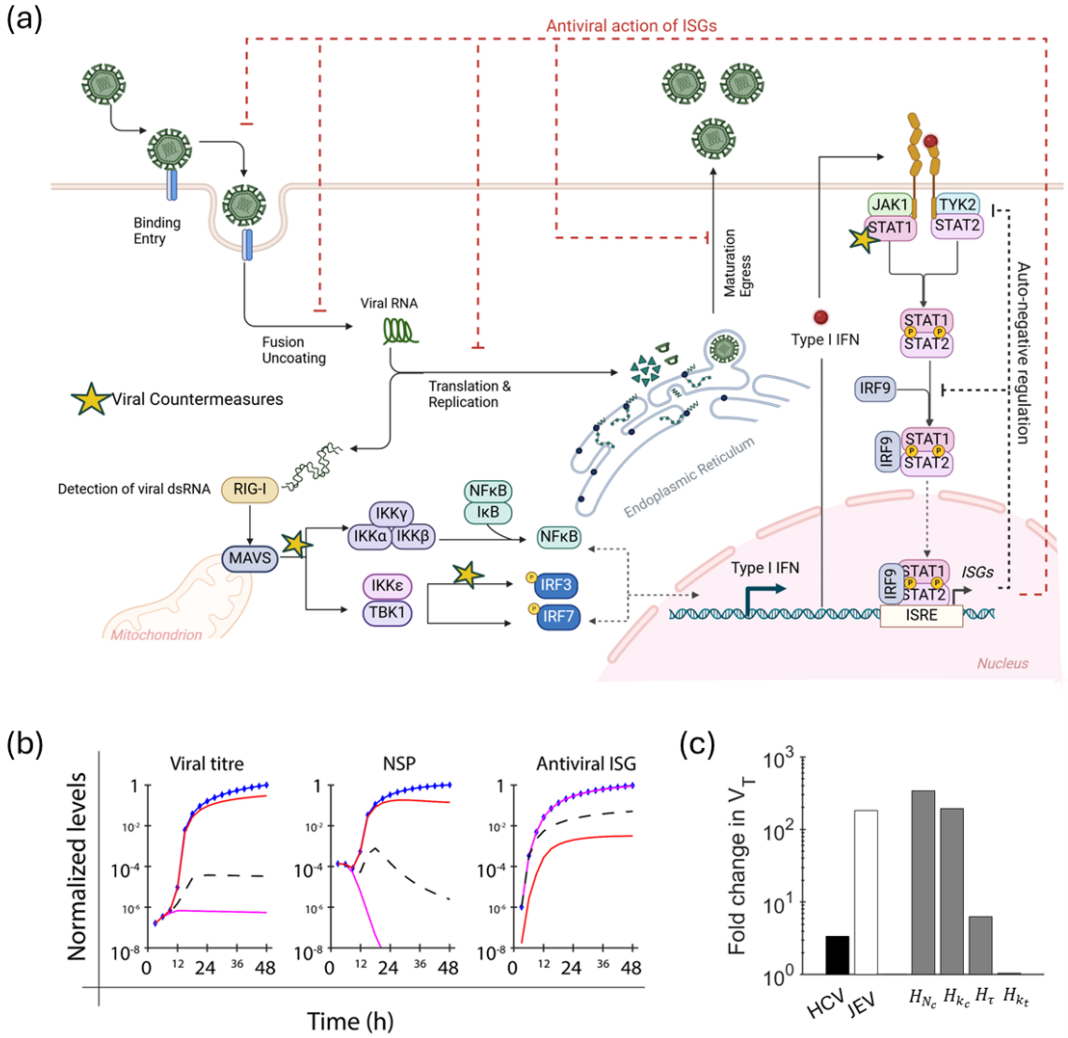

Figure 1: **Integrated mathematical model of the viral life cycle with interferon pathways** Schematic representation of the intracellular model coupling the (+)RNA virus life cycle with host innate immune signalling. Viral infection begins with extracellular virions (V_E) binding and entering the host cell, followed by uncoating and release of viral RNA. This RNA undergoes translation to produce structural (P_S) and non-structural proteins (P_{NS}), and replication via a double-stranded RNA intermediate (RC_{CM}), often sequestered within membrane compartments to evade immune detection. Leakage of replication intermediates into the cytoplasm (R_{ds}) can trigger recognition by pattern recognition receptors like RIG-I, activating the MAVS and downstream transcription factors such as IRF3 and NF-κB. This results in the production and extracellular release of type I interferons. Extracellular IFN-I binds to its receptor activating the JAK-STAT signaling cascade via STAT phosphorylation, which induces the transcription of interferon-stimulated genes (ISGs). These include antiviral ISGs (ISG_{av}) that inhibit viral processes (effect strength, $I_{V,N}$), positive regulators, and negative regulators involved in feed ack control of the immune response. Viral countermeasures, particularly via non-structural proteins, can suppress the activity of antiviral ISGs (suppression strength, $V_{I,N}$). b) Simulated dynamics comparing the effect of virus-immune interactions on the dynamics viral titer (left), non-structural protein levels (middle), and antiviral ISGs (right), normalized to steady-state levels in the no-interaction base-line represented by the blue line (S_0: $I_{V,N} = I_{I,N} = V_{I,N} = 0$). The red line depicts the fully interacting system (S_1: $I_{V,N} = I_{I,N} = V_{I,N} = 1$). The magenta line indicates immune activation alone (S_b: $I_{V,N} = 1$, $I_{I,N} = V_{I,N} = 0$). The black dashed line shows the scenario with host immune activation and feedback regulation but no viral immune suppression (S_1: $I_{V,N} = I_{I,N} = 1$ and $V_{I,N} = 0$). These results demonstrate how the balance of immune regulation and viral countermeasures determines infection dynamics. c) Fold change in total viral titer (V_T) between the no-interaction base case (S_0) and the full virus-immune interaction scenario (S_1) for HCV (black bar), JEV (empty bar), and a few hypothetical viruses (grey bars). All the model parameter values of the hypothetical virus, H_θ, are based on HCV parameter values, except for θ which is based on JEV's θ value. θ was restricted to N_C, k_c, τ and k_t because HCV and JEV primarily differ in these parameters.

the innate immune system impedes the viral life cycle and itself ($I_{V,N} = I_{I,N} = 1; V_{I,N} = 0$), and finally (d) S_1, where all interplays are considered ($I_{V,N} = V_{I,N} = I_{I,N} = 1$).

Compared to S_0 (blue line, Figure 1b), the levels of viral non-structural proteins (NSP, Figure 1b center panel) and titre Figure 1b left panel) drop significantly in the presence of the antiviral effect ($I_{V,N} = 1$, magenta line, Figure 1b). The reduction is less and delayed when negative auto-regulation of the immune pathway is also considered (black dashed line, Figure 1b). However, this reduction is almost nullified when viral countermeasures on the antiviral effect of the immune response is also considered (red line, Figure 1b). Furthermore, in the case of the dynamics of interferon-stimulating genes (ISG), the levels peaked in the presence of the antiviral response alone, reinforcing the role of innate immunity in suppressing viral propagation. The addition of immune self-regulation led to a noticeable decline in ISG levels, and their expression dropped to minimal levels when viral counteraction was also active (Figure 1b).

We simulated the model for the Japanese Encephalitis Virus (JEV) by adjusting the viral parameter values [19]. The system kinetics are qualitatively similar to those of HCV (SI Figure 1); however, notable differences were identified when comparing the steady state values across different scenarios. The ratio of viral titre at steady state between S_0 and S_1 is 3.36 for HCV and 182.6 for JEV (Figure 1c). We hypothesize that this observation can be attributed to the faster formation (higher k_c) and higher number of replication complexes (higher N_C) in the case of the JEV life cycle. The quicker and higher accumulation of replication intermediates, driven by these parameters, facilitates earlier and stronger immune activation; so when the antiviral action of immune response is considered (S_1) the reduction in viral titre is more in the case of JEV compared to HCV.

We verify this, we constructed a series of hypothetical viral strains, denoted H_θ. The viral parameter values of H_θ are identical to those of HCV, except for the parameter θ, which was set to the corresponding JEV value. We restricted the set of substituted parameters to N_C, k_c, τ, and k_t, as HCV and JEV primarily differ in the values of these parameters. Among the resulting hypothetical viruses, we see that H_{N_C} and H_{k_c} show the highest fold-change, akin to JEV, supporting our hypothesis of a faster and stronger activation of innate immmune response (akin to [37]). Perturbing the delay in compartment formation (τ) in HCV doesn't seem to alter the fold change. However, as we increase the viral translation rate (k_t) of HCV, the viral titre doesn't change between S_0 and S_1 scenarios (as for H_{k_t}, Figure 1c). We reason that the faster and higher production of viral proteins leads to a stronger suppression of the innate immune response and its effect on the viral life cycle.

The virus-immune interactions result in bifurcation in system behaviour

To better capture the nuanced effect of virus-immune interactions, we varied the corresponding strengths in a spectrum rather than just switching them on and off. Upon varying the strength of immune action

on the viral life cycle ($I_{V,N}$) and viral countermeasures on immune response ($V_{I,N}$), we observe a sharp transition in the HCV viral load (Figure 2a). Specifically, when $I_{V,N}$ is fixed at 1, the system shifts from an 'ISG-high, virus-low' state to an 'ISG-low, virus-high' state as $V_{I,N}$ exceeds 0.44. The points on the $I_{V,N} - V_{I,N}$ plane where the behavior transition occurs are called bifurcation/critical points, marked by $(I^*_{V,N}, V^*_{I,N})$. This transition as well as the orientation of the bifurcation front (the front formed by the bifurcation points) in the $I_{V,N} - V_{I,N}$ plane (Figure 2b, top panel) reflects the antagonistic dynamics between antiviral signaling and viral countermeasures.

A similar qualitative pattern is observed for JEV (Figure 2b, bottom); however, for the same fixed $I_{V,N}$, the critical threshold of $V_{I,N}$ required for state transition is lower for JEV than for HCV. For instance, at $I_{V,N} = 1$, the threshold value, $V^*_{I,N}$, is 0.281 for JEV, compared to 0.44 for HCV. The lower threshold observed for JEV likely reflects its rapid rate of protein synthesis, which facilitates the earlier deployment of viral countermeasures to suppress the host immune response. In contrast, HCV, characterized by slower protein production, necessitates more potent countermeasures to achieve comparable immune suppression.

We next identify which viral and immune processes have the maximum impact on the bifurcation front. Thus, we assessed the relative sensitivity (using the finite difference method; details in methods) of the critical strengths of innate response and viral countermeasures towards changes in model parameter values. An immediate observation is the inverse correlation between the parameter sensitivity coefficients of $I^*_{V,N}$ and $V^*_{I,N}$, highlighting the antagonistic nature of the two interactions. Further, we observe that parameters that accelerate or increase viral protein production, directly (through viral translation) or indirectly (by increasing viral RNA levels through replication), have the highest influence on the value of $V^*_{I,N}$, and consequently on $I^*_{V,N}$. Furthermore, viral and host processes that lead to the detection of dsRNA (such as the production of viral dsRNA replication intermediate) or the increase in the levels of immune effectors (such as ISG production and degradation rates) significantly impact the value of $I^*_{V,N}$ and thus on $V^*_{I,N}$.

We further investigated the influence of these parameters on the bifurcating front, specifically, how the front changes when these parameter values are varied. Except for the k_c, changes to values of these parameters lead to an approximately parallel shift of the bifurcation front (Figure 2d and SI Figure 2). For example, doubling the translation rate of host ISG RNA leads to an approximate five-fold increase in $V^*_{I,N}$ for HCV, independent of the value of $I^*_{V,N}$ used for simulation. In contrast, the fold-change in the value of $V^*_{I,N}$ upon a perturbation in k_c is conditioned on the value of $I_{V,N}$ used. As the value of k_c is doubled, the fold-change in value of $V^*_{I,N}$ increases from 1 (no change) at low $I^*_{V,N}$ to as high as 12 at high $I^*_{V,N}$ (Figure 2d insets). This strange dependence can be attributed to k_c governing the kinetics of production of viral dsRNA, a molecule that both fuels the viral life cycle (pro-viral) and triggers the immune response (pro-immune). We posit that at low values of $I_{V,N}$, the pro-viral and pro-immune

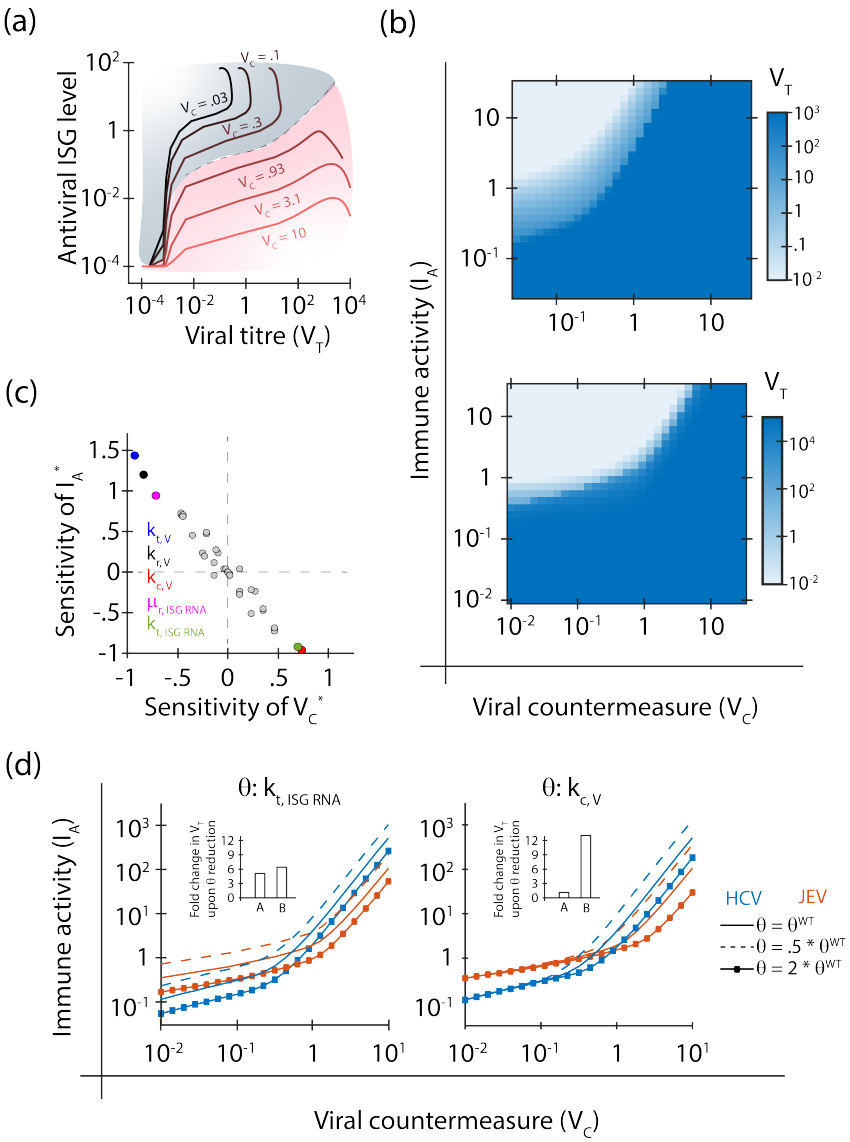

Figure 2: **Bifurcation structure and sensitivity analysis reveal critical control points in infection dynamics**
(a) The phase plot showing the dynamics of viral titre and Antiviral ISG levels during a hepatitis C virus infection is shown for different values of viral countermeasure strengths ($V_{I,N}$). The system shifts from a 'virus-high, ISG-low' state to a 'virus-low, ISG-high' state as the value of $V_{I,N}$ increases, with the transition happening at $V_C = V_C^* = 0.4$. (b) The heatmap of the viral titer output (V_T) during HCV (top) and JEV (bottom) infection is shown as a function of $V_{I,N}$ and immune action strength ($I_{V,N}$) Darker shades indicate higher viral loads, highlighting the nonlinear response of viral output to changes in host-virus interaction parameters. (c) Scatter plot showing the parameter sensitivity indices of critical values (corresponding to bifurcation) of $I^*_{V,N}$ and $V^*_{I,N}$. Colored dots denote the most influential parameters: $k_{t,V}$, $k_{r,V}$, $k_{c,V}$, $\mu_{r,ISGRNA}$ and $k_{t,ISGRNA}$ (Description in Supplementary Table S). (d) The bifurcation fronts for HCV blue) and JEV (orange) infection systems are shown for different values of $k_{t,ISGRNA}$ (translation rate of ISG mRNA, left) and $k_{c,V}$ (compartmentalization rate of viral dsRNA, right). The solid line, dashed line and the solid line with square symbols show the bifurcation front when the value of the parameter of interest is unperturbed, reduced by half, and doubled, respectively. The insets show the fold change in the steady state values of HCV V_T when the corresponding parameter values were reduced by 50% at two points chosen along the front - A: $V_C = .398, I_A = .211$ and B: $V_C = 3.98, I_A = 74.47$. V_c - Viral Countermeasures ($V_{I,N}$)

benefits obtained by increasing k_c almost cancel each other leading to minor changes in system behavior and thus in the value of $V^*_{I,N}$. However, increasing the value of k_C when the value of $I_{V,N}$ is high implies that viral dsRNA is formed fast, triggering the strong immune response very soon after the infection. The early triggering of the strong immune action would require stronger viral countermeasures, leading to a significant shift in the front when $I_{V,N}$ is high (Figure 2d).

These findings reveal that small shifts in host immunity or viral strategies can determine infection outcomes, highlighting key host-virus interactions. Sensitivity analysis identified critical parameters, including replication complex formation, as potential broad-spectrum antiviral targets.

Time-Resolved Pathway Analysis Reveals Dynamic Immune Responses to Viral Infection

To gain deeper insights into system behaviour, we clustered model variables based on the similarity in their temporal dynamics over a 48-hour infection period (Figure 3, top panel). Hierarchical clustering of z-normalised trajectories revealed distinct modules comprising of viral molecular species and host immune signalling components that are co-regulated during the course of infection. To illustrate these patterns, we plotted the average normalised trajectories of variables within each cluster, revealing the modular and time-structured nature of the host response (Figure 3b, individual plots in SI Figure 3).

We observed that various intracellular viral components - including viral RNAs and proteins - as well as immune sensors involved in viral recognition (dark blue nodes, Figures 3a and 3c), exhibit highly correlated dynamics. These components constitute the "viral molecules and immune detection" cluster, characterized by a gradual increase in their levels, which peaks around 20 hours post-infection (hpi), followed by either saturation or a slow decline in levels (dark blue line, Figure 3b). The tight correlation among viral molecular species is consistent with their coupled synthesis. The viral double-stranded RNA (dsRNA), which serves as the viral replication intermediate and the primary immune trigger, most likely mediates the high correlation between the dynamics of viral molecules and upstream immune signaling factors.

Upstream signaling cascades lead to the activation, phosphorylation, or translocation of specific host proteins. The native (unmodified) forms of these proteins seem to group together in the "Native form" cluster (violet nodes, Figure 3a,c). Their levels initially decline, likely due to activation-related consumption or complex formation, followed by a partial recovery (violet line, Figure 3b). Correspondingly, their activated and phosphorylated counterparts—comprising the "Activated intermediate" cluster (light blue nodes and lines, Figure 3)—show a rapid increase, peaking around 12 hpi. This cluster includes factors such as aMAVS, aIKK, and pTBK1, which mediate further downstream transcriptional responses, including IRFs activation and ISG expression. Factors in "RTC-TYK" cluster (green nodes, Figure 3) display a biphasic but overall declining pattern. This is due to their continuous consumption for the

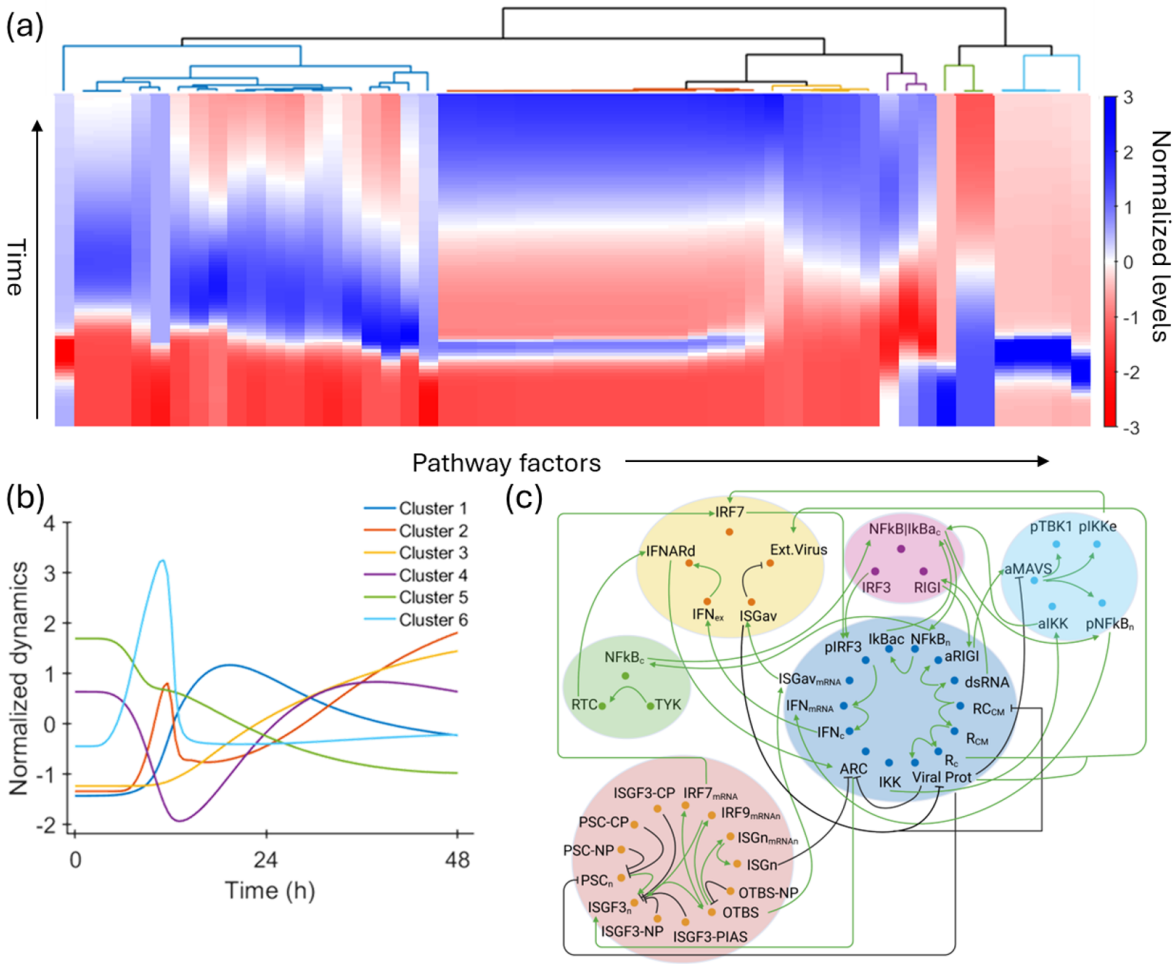

Figure 3: **Norm lized dynamics based cluster analysis**
(a) The heatmap shows the normalized expression levels of pathway factors over time, clustered using hierarchical clustering. Distinct clusters are indicated by the dendrogram. (b) The mean temporal profiles of each cluster, depicting the characteristic dynamic behavior of grouped components across the 48-hour time course, are plotted. (c) Schematic representation of intra- and inter-cluster interactions among pathway components, illustrating the flow of information from upstream sensors to downstream effectors and the regulatory crosstalk between clusters.

activation of transcription factors of downstream immune effectors. Negative regulation also contributes to this decline, suggesting its importance in activating downstream signalling, the JAK-STAT pathway.

Factors in the "IRF-ISG" cluster (orange nodes, Figure 3) display a transient rise in levels, following the activation peak of the intermediate signaling factors. However, critical members of this group, such as aMAVS and PSCn, are subsequently downregulated by viral countermeasures. This leads to a decline in their expression, along with associated correlated variables. Additionally, negative feedback within the immune system itself contributes to this downregulation. The "IRF-ISG" cluster ultimately leads to the production of "downstream immune effectors" such as IRF7 and IFN (yellow nodes, Figure 3), which show a slower yet sustained increase in levels. Interestingly, viral particles also fall into this group due to a similar progressive increase in abundance.

Overall, this temporal clustering approach, contextualised by pathway knowledge, provides a nuanced view of the coordinated dynamics underlying host-virus interactions.

Dose-Dependent IFN Desensitization Is Mediated by Eeceptor-Kinase Complex and TYK Dynamics

Having examined the molecular and pathway-level responses to viral infection, we next focused on the signaling cascade elicited by interferon (IFN) treatment. Specifically, we investigated the mechanistic basis of IFN desensitization - a phenomenon wherein sustained or repeated IFN exposure diminishes cellular responsiveness.

Our model captures the dose-dependent desensitization effect. When cells are initially treated with a high dose of IFN (100 nM), we observe a sharp induction of interferon-stimulate gene (ISG) expression; the ISGn mRNA and ISGav mRNA levels rapidly rise to 0.75 and 140 units, respectively (Figure 4 a and b). However, this activation is transient; both markers decrease substantially, stabilizing around 0.01 and 60 within 24 hours. Notably, when a second dose of 100 nM IFN is administered 24 hours after the first, no further induction of ISGn or ISGav mRNA is observed, indicating complete desensitization. In contrast, when the first dose is reduced to 1 nM, followed by a second high dose (100 nM), a modest re-induction of both ISGn and ISGav is evident, suggesting partial desensitization. These trends are consistent with experimental reports of dose- and time-dependent IFN desensitization.

We evaluated the chi-squared metric, the sum of squared of differences in the normalized dynamics of each variable under (D1, D2) = (1 nM, 1 nM) and (1 nM, 100 nM) IFN exposures. The variables showing the largest divergence were TYK2 and the receptor-kinase complex, while most other species, including downstream transcription factors and ISGs, displayed minimal deviation (Figure 4 c and d). Interestingly, TYK2 and the receptor complex had also clustered together in our earlier modular analysis (green cluster, Figure 3) reinforcing their shared regulatory role. Our predictions are consistent with reported biology, as the activity of receptor-kinase complex, which comprise of the IFN receptors (IFNAR1/2) and associated

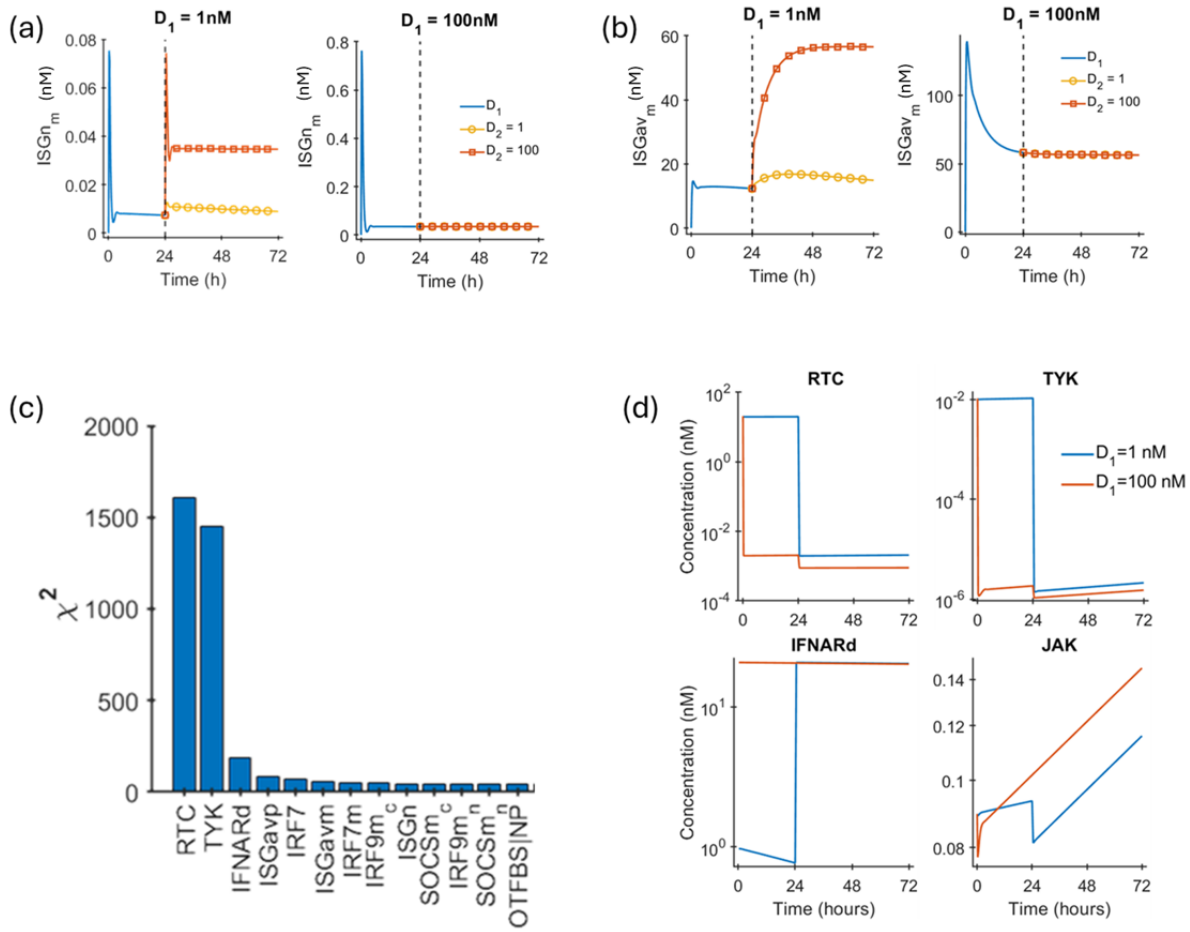

Figure 4: **Dose-dependent sensitization of the JAK-STAT pathway**
The kinetics of (a) an upstream ISG transcript involved in immune suppression (ISG_n), and (b) a downstream ISG transcript involved in viral suppression (ISG_{av}), are shown for two two-dose interferon (IFN) treatments. Two priming conditions are compared: an initial low dose of 1 nM IFN followed by a 100 nM boost after 24 h (Condition 1, left panels), and an initial high dose of 100 nM IFN followed by a 100 nM boost after 24 h (Condition 2, right panels). (c) The χ^2 values (see Methods), used to quantify the deviation in dynamic trajectories between the two IFN conditions, are plotted. Few of the top-ranking species, indicating model components most sensitive to initial IFN dose, are shown. (d) Time-course dynamics of model species with the two highest (RTC, TYK) and two moderate ($IFNARd$, JAK) χ^2 values are shown, demonstrating IFN dose-dependent differences in system response.

kinases (TYK2 and JAK1) and serve as the entry point for JAK-STAT pathway activation, is tightly regulated by negative feedback mechanisms [38, 39, 40]. The feedback is induced in a dose-dependent manner, with high IFN doses triggering rapid expression and accelerated turnover of receptor and kinase.

Timing and Dosage of IFN Treatment Critically Shape Antiviral Efficacy, Enhanced by Targeting Viral Lifecycle Processes

We next investigated the impact of interferon (IFN) administration as a prophylactic or therapeutic intervention, focusing on how the timing and dosage of IFN influence disease progression (Methods). Simulations reveal that IFN treatment significantly reduces viral load in a dose-dependent manner when

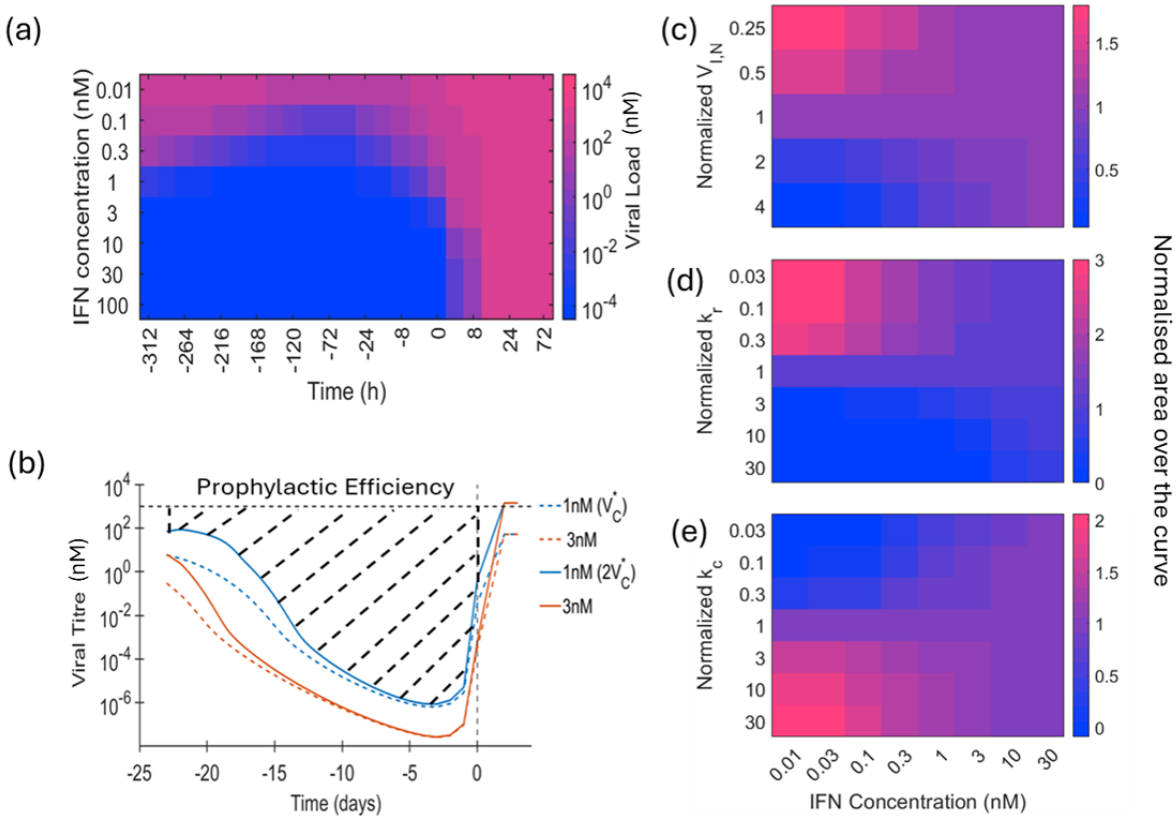

Figure 5: **Exploring IFN: From Preventive Strategies to Therapeutic Interventions**
(a) A heatmap of viral load as a function of the timing and dose of IFN treatment is shown. Simulations were performed with viral countermeasure efficiency set to twice the critical threshold ($V_{I,N} = 2V^*_{I,N}$). (b) Line plots of viral load over time for two IFN concentrations (blue: 1 nM, red: 3 nM) and two levels of viral countermeasure efficiency (dotted lines: $V_{I,N} = V^*_{I,N}$; solid lines: $V_{I,N} = 2V^*_{I,N}$) are shown. To calculate the prophylactic efficiency, we evaluate AOC (see Methods): the area between the viral load curve and a nominal horizontal line (dashed black line) as shown here. A stronger prophylactic action would lower the viral titer, thereby increasing the AOC value. (c) The heatmap shows how the prophylactic efficacy (given by the normalised area over the curve, or nAOC) varies as a function of IFN concentrations and viral countermeasure efficiencies ($V_{I,N}$). (d) The heatmap shows how the prophylactic efficacy (given by nAOC) varies as a function of IFN concentrations and viral replication rate (k_r, V). (e) The heatmap shows how the prophylactic efficacy (given by nAOC) varies as a function of IFN concentrations and viral compartmentalization rate ($k_{c,V}$).

administered before or within a narrow window shortly after infection (Figure 5a). However, the timing of addition is more important in determining treatment efficacy For instance, a low IFN dose (0.3 nM) administered 1–7 days prior to infection confers a greater antiviral effect (>100 times higher) than a high dose (>10 nM) applied just a few hours post-infection (top left panel). IFN loses its antiviral potency when applied 8 hours or more after infection, consistent with earlier experimental findings [41, 42, 43].

Prompted by this observation, we hypothesized that IFN could act as an effective prophylactic agent. We used our virus–immune interaction model to study IFN-prophylaxis (Figure 5b) and combination treatments involving IFN and direct-acting antivirals (targeting key viral life cycle steps such as replication, compartmentalization, and countermeasure mechanisms, Figure 5c-e). Given the difficulty of precisely predicting infection timing in real world settings, we quantified antiviral efficacy by integrat-

ing the steady-state viral load across a range of IFN pre-treatment timings. This was done using an area-over-curve (AOC) metric (see Methods), with higher AOC scores indicating greater antiviral suppression. We further normalized the metric (nAOC) by subtracting the AOC of the unperturbed system, evaluated the fold enhancement. The results (bottom panels) show that increasing the dose of IFN or reducing the effectiveness of viral countermeasures ($V_{I,N}$, Figure 5c) or viral replication rate (k_r, Figure 5d) enhances prophylactic efficacy (i.e, higher nAOC). In particular, accelerating the formation of replication compartments (k_c, Figure 5e), which we previously identified as a key bottleneck, also improves the efficacy of IFN, possibly due to earlier recognition and activation of antiviral pathways. Effect of other parameter variations on IFN prophylaxis is shown in SI Figure 4.

Collectively, these findings underscore the importance of early IFN exposure in prophylaxis and demonstrate how modulating viral lifecycle parameters can synergize with innate immunity to enhance antiviral protection.

Discussion

The integrative approach of our model by combining detailed representations of the viral life cycle and innate immune signaling pathways, enables a more comprehensive understanding of virus-host interactions. Prior models predominantly concentrated on either viral replication or pure immune system modeling, often neglecting the specifics of either the immune signaling networks' influence on various stages of the virus life cycle or the impact of viral suppression on host pathways [17, 22, 44, 30]. By incorporating the RIG-I/MAVS, JAK-STAT, and ISG pathways, along with processes like dsRNA-triggered immune activation and viral countermeasures on the host immune pathways, we have attempted to model the dynamic feedback loops and molecular crosstalk that define the balance between viral replication and immune defense, thus facilitating a more accurate representation of host-virus interactions. This has allowed the identification of critical bifurcation points in infection outcomes, such as transitions between "virus-high, ISG-low" and "virus-low, ISG-high" states, and introduced the notion of thresholds that govern this transition. Such cellular bimodality in infection has been observed in single-cell experiments as well [27, 13, 45, 46] (reviewed in [47]). Similarly, while previous phenomenological models [31, 12, 31, 28, 26, 48] were able to propose the two opposing outcomes during viral infection, now we are able to pin-point the viral and host processes that strongly influence this delicate balance. Insights derived from our molecularly informed model can guide the design strategies for effective Direct-Acting Antivirals (DAAs), Host-Targeting Antivirals (HTAs), and their combinations.

Another key outcome of such molecular-level analysis is the ability to recapitulate IFN desensitisation under repeated exposure to IFN in a dose-dependent manner. For example, our model identifies IFN receptor–associated kinases, particularly TYK2 and Receptor-TYK2 Complex (RTC), as key molecules

mediating IFN-desensitization. This is consistent with the experimental evidence that shows that TYK2 is essential for type 1 IFN signalling, leading to the activation of the STAT pathway [49, 50, 51]. Prolonged or frequent IFN exposure results in a decrease in receptor accessibility and an amplification of SOCS-driven negative feedback at the receptor-tyrosine complex (RTC). This process occurs as IFN engagement activates the TYK2 kinase associated with receptors and subsequently leads to desensitization [52, 7, 40]. These observations underscore the pivotal role of TYK2/RTC in modulating IFN sensitivity.

By incorporating dsRNA dynamics and their role in triggering RIG-I signaling, the model is also able to elucidate the importance of early immune activation and the trade-offs between viral replication and immune detection. This integrative framework helps explain the differential immune stimulation and responses by different viral infections. We propose that extent of replication compartment formation and kinetics of dsRNA compartmentalisation are key factors that can drive a more rapid and robust innate immune response. Our predictions are consistent with the early induction of IFN observed for JEV infection, where replication compartment characteristics have been attributed as the responsible feature of JEV [37, 53]. Thus, the molecular-level details in our model can enable comparative analysis across classes of (+)RNA viruses, offering mechanistic insights into how viral replication and lifecycle modulates innate immune activation.

Furthermore, the use of time-resolved clustering to analyze condition-specific temporal patterns in immune signaling has revealed potential markers for infection states and therapeutic efficacy. For instance, pathway components exhibiting similar dynamics may reflect co-regulation within shared transcriptional programs or regulatory circuits. The identification of such co-dynamic clusters can highlight temporal coordination and facilitate model simplification through coarse-graining, allowing groups of functionally related variables to be analysed as unified modules. Moreover, these clusters of temporally co-varying molecules may serve as dynamic biomarkers of infection progression or treatment response, or disease outcome, providing mechanistic insight and potential translational utility.

We extend our model to report a framework for estimating the prophylactic efficiency of IFN against HCV infection. We show that low-dose prophylactic administration of IFN can considerably inhibit viral replication, surpassing effectiveness of high-dose treatment post-infection. Thus, interventions employing IFN prophylactic treatment, especially in high-risk populations or during outbreaks, could be a viable opportunity. Similarly, our model suggests the ineffectiveness of IFN treatment beyond a critical interval post-infection. For example, we observe a complete loss of IFN antiviral action at eight hours post-infection for a slow-growing virus like HCV. This is consistent with previous experimental studies on RNA strand RNA viruses like SARS-CoV-2 and dengue, where delayed IFN treatment was shown to be ineffective or even detrimental [41, 42, 43]. Our findings contribute to a growing body of work suggesting that the timing and dosage of immune interventions can strongly influence disease outcomes [54].

Our framework also allows us to evaluate which drug combination strategies, including those targeting

viral processes and inherent antagonistic feedback loops, can significantly enhance IFN prophylaxis. For example, antivirals targeting viral replicase complex, translation, or virus-mediated suppression of immune pathways augment the action of IFN dose. However, a reduction in the formation of dsRNA intermediates can decrease immune detection and hence reduce the effectiveness of IFN pretreatment, suggesting a nuanced trade-off between viral replication and immune detection. In the future, our approach can be employed to inform virus-specific IFN strategies.

Our model simplifies innate immune signaling by focusing on a single class of pattern recognition receptors (PRRs) and assuming average cellular behavior. While multiple classes of PRRs (TLRs, RLRs, NLRs, CLRs) are involved in shaping innate immune responses, it is established that viral dsRNA is a principal trigger of antiviral responses [55, 56]. Accordingly, our model focuses on dsRNA-sensing pathways, which are central to detecting RNA virus infections. To simplify the interpretation of innate immune feedback, we employed uniform negative feedback across signaling nodes, overlooking context-dependent regulators like SOCS proteins, which can vary by cell type and stimulus. However, our model explicitly allows us to specify such molecular-level control by virtue of the independent parameters defined for such interactions. In the future, our model can serve to examine the individual role of such interactions explicitly. We also chose to depict the action of antivirals as a reduction in the corresponding viral parameter, although integrating the pharmacological drug profiles would improve predictions of the dynamic outcomes of the infection. Despite simplifications, our framework lays a robust foundation for studying molecular process specific antiviral responses, offering flexibility for refinement and validation. The ability of our model to accommodate the broad molecule-level interactions and nuisances also allows us to incorporate cellular- and tissue-level heterogeneity. Combined with spatio-temporal dynamics and multi-cell immune responses, one can extend our model for understanding viral infection dynamics in complex tissue.

Collectively, our study provides a universal predictive framework for mapping the interactions between host immune networks and viruses that shape the outcome of infections and how therapeutic interventions can be combined and optimised more effectively by targeting virus vulnerabilities or reinforcing host defences. In spite of its reductionist approach, our results highlight the importance of early immune activation, ISG dynamics, fine-tuned IFN signaling, and virus life cycle dynamics in defining the outcome of the tug-of-war between the virus and the host cell.

Methods

Models integration and extension

To create a detailed, mechanistic model of the virus-innate immune response, we combined the existing detailed intracellular virus life cycle model by Chhajer et al.[19] with another existing RIGI-IFN-ISG

model by Burkart et al.[36]. A few model variables, parameters, and equations were added to enable this integration and to incorporate some key steps missed by these models. The model equations are mentioned in the SI file.

Viral life cycle and dsRNA detection

We added the following variables and equations to the viral life cycle model proposed by Chhajer et al.[19] to incorporate the extracellular viral dynamics of viral entry and internalization:

$$\frac{dV_0}{dt} = -k_{\text{en}} \cdot V_0 \tag{1}$$

$$\frac{dV_I}{dt} = k_{\text{en}} \cdot V_0 - k_f \cdot V_I - \mu_{V_I} \cdot V_I \tag{2}$$

Subsequently, the equation monitoring the levels of cytoplasmic viral RNA is changed:

$$\frac{dR_{\text{cyt}}}{dt} = k_e \cdot R_{\text{CM}} - k_a \cdot P_S \cdot R_{\text{cyt}} - \mu_r \cdot R_{\text{cyt}} - \text{RC}_{\text{form_rate}} + \mathbf{k_f} \cdot \mathbf{V_I} \tag{3}$$

Viral entry was modelled as a first-order process governed by the rate constant k_{en} (akin to [30]) (Equation 1). Internalized virus (V_I) accumulates at this rate and can either uncoat at a rate k_f or be degraded at a rate μ_{V_I} (Equation 2). Upon uncoating, the viral RNA is released into the cytoplasm, contributing to the cytoplasmic viral RNA pool (R_{cyt}). The dynamics of R_{cyt} are governed by Equation 3, where the input from uncoating ($k_f \cdot V_I$) has been incorporated. All other terms in this equation remain unchanged from the original model by [19]. Similarly, ODEs describing the dynamics of structural and non-structural viral proteins (P_S, P_S), replication compartment formation (RC_{form_rate}), and replication complexes within compartments (RC_{CM}) are retained from the original framework.

The previous model [19] did not accommodate the leakage of dsRNA into the cytoplasm; however, this process is critical as cytosolic dsRNA acts as a key trigger of the innate immune response. Therefore, we explicitly include it in our model, the leakage of double-stranded RNA (dsRNA) from the replication compartments into the cytosol at the rate of a_{RC} (akin to [30]) and the subsequent initiation of RIG-I signalling. The cytosolic dsRNA is subject to natural degradation at rate μ_r, is replenished due to the deactivation of RIG-I at b_{RIGI}, and is cleared via RIG-I–mediated sensing, which depends on the concentrations of both RIG-I and dsRNA at a rate of k_{RIGI}. This serves as the link between the viral life cycle and the RIGI pathway.

$$\frac{d\text{RNA}_{\text{ds}}}{dt} = a_{\text{RC}} \cdot \text{RC}_{\text{CM}} - \mu_r \cdot \text{RNA}_{\text{ds}} + b_{\text{RIGI}} \cdot \text{aRIGI} - k_{\text{RIGI}} \cdot \text{RIGI} \cdot \text{RNA}_{\text{ds}} \tag{4}$$

Innate immune signaling pathway

The innate immune model by [36] did not include the dynamics of Interferon Regulatory Factor 7 (IRF7), a key transcription factor involved in type I interferon (IFN) gene induction, particularly in plasmacytoid dendritic cells and during late-phase antiviral responses [57] and is responsible for the induction of the IRF7 gene [58]. Due to the high degree of homology between IRF3 and IRF7, we assumed that IRF7 undergoes phosphorylation via a mechanism analogous to that of IRF3, and modelled it as shown below:

$$\frac{d\text{IRF7}}{dt} = k_{71} \cdot \text{Vn2c} \cdot \text{pIRF7} - \text{IRF7} \cdot k_{\text{IRF3_IKKe_TBK1}} \cdot (\text{pIKKe} + \text{TBK1}) + k_{79} \cdot \text{IRF7_m} - \text{deg} \cdot \text{IRF7} \quad (5)$$

$$\frac{d\text{pIRF7}}{dt} = \text{IRF7} \cdot \text{Vc2n} \cdot k_{\text{IRF3_IKKe_TBK1}} \cdot (\text{pIKKe} + \text{aTBK1}) - k_{71} \cdot \text{pIRF7} \quad (6)$$

Phosphorylation of cytoplasmic IRF7, mediated by TBK1 and IKKϵ, drives its activation and nuclear translocation. This is governed by $k_{\text{IRF3_IKKe_TBK1}}$, and once in the nucleus, pIRF7 can be dephosphorylated or exported back to the cytoplasm, a process captured by a first-order term with rate constant k_{71}. IRF7 is produced via translation from its IFN-dependent induced mRNA, controlled by the translation rate constant k_{79}. Finally, IRF7 is subject to constitutive degradation with a first-order decay rate, *deg*.

Incorporation of feedback at multiple levels by both the virus and innate immune system

Interferon-stimulated g nes (ISGs) play a crucial role in the antiviral defence against *Flaviviridae* viruses by targeting various stages o the viral life cycle. For example, the ISG MX1 inhibits viral replication by disrupting viral RNA synthesis, while viperin interferes with the assembly of the virus by disrupting the viral envelope formation. Collectively, these ISGs form a multifaceted defence mechanism by targeting viral entry, replication, translation, assembly, and release, highlighting the complexity and effectiveness of the host antiviral response against *Flaviviridae* viruses ([7, 8, 20].

As a countermeasure, *Flaviviridae* viruses have evolved strategies to inhibit the host innate immune response at multiple stages. They antagonise interferon (IFN)-induced antiviral state by targeting both the RIG-I-like receptor (RLR) pathway and the downstream JAK-STAT signalling cascade. By interfering with these pathways, *Flaviviridae* effectively suppress type I IFN production and signaling, thereby enhancing viral replication and persistence [59, 60, 61].

In addition to viral countermeasures, the host immune system also incorporates intrinsic negative feedback mechanisms to regulate and resolve inflammatory signalling, thereby preventing excessive immune activation and tissue damage. While the role of negative regulators such as SOCS (Suppressor of Cytokine Signaling) proteins has been previously considered, here we lump the actions of multiple regulatory molecules—including USP18, which is rapidly induced upon IFN signaling and attenuates the

JAK-STAT pathway [38, 39, 24]—into a unified negative feedback term.

To quantitatively capture the dynamics of these interacting viral and host feedback systems, we introduced three lumped/hyper parameters (pseudo-variables) representing distinct functional arms of the system: $V_{I,N}$ (efficacy of viral immune antagonism), $I_{V,N}$ (potency of ISG-mediated antiviral activity), and $I_{I,N}$ (efficiency of host negative regulation of immune signalling). These components are integrated into a generic rate modulation function as follows:

$$k_i' = \frac{k_i}{1 + \rho[A]} \tag{7}$$

and the degradation rates μ_i are changed as

$$\mu_i' = \mu_i(1 + \rho[A]) \tag{8}$$

Here, k_i denote the intrinsic rate constant for a particular process of viral life processes- viral entry (k_{en}), fusion (k_f), replication (k_r), translation (k_t) and egress (k_a), μ_i denotes the degradation processes - degradation of viral RNA (μ_r), dsRNA (μ_r) and proteins (μ_p) and immune processes - MAVS activation (k_{MAVS}), activation of IRF3 and IRF7 ($k_{IRF3_IKKe_TBK1}$) and activation of activated receptor complex (ARC) (k_{13}), while ρ corresponds to one of the modulation coefficients $V_{I,N}$, $I_{V,N}$, or $I_{I,N}$, depending on the process under consideration. The variable $[A]$ represents the concentration of the modulating protein, such as an antiviral protein ($ISGav$), a viral non-structural protein (P_{NS}).

Calculation of critical values and sensitivity Analysis

To identify the critical value of $V^*_{I,N}$ (or $I^*_{V,N}$), we systematically vary one of $V_{I,N}$ or $I_{V,N}$ keeping the other fixed, and record the extracellular viral concentration at 48 hours post-infection (V_{ext}). Next, we evaluate the first-order numerical derivative of the logarithm of viral output ($log_{10}(V_{ext})$) with respect to the variable varied and identify the point of maximum change as the critical value. $V_{I,N}$ and $I_{V,N}$ were varied in the logarithm scale to span a large dynamics range.

To evaluate the sensitivity of the thresholds ($V^*_{I,N}$ and $I^*_{V,N}$) on model parameter 'i', we vary the value of the 'i^{th}' model parameters (θ_i), evaluate the new threshold values and calculate the sensitivity index using the following equation:

$$SI = \left(\frac{\Delta V^*_{I,N}}{V^*_{I,N}}\right) \Big/ \left(\frac{\Delta\theta}{\theta}\right) \tag{9}$$

Here, a five-point central difference formula was used to calculate the change in the threshold values. The threshold values were evaluated at $\theta_i = [0.9, 0.95, 1, 1.05, 1.1] \times \theta_i^0$, where θ_i^0 is the nominal value of the parameter where the sensitivity is evaluated. Here we fix $V_{I,N}$ at 0.444 to evaluate $I^*_{V,N}$, and fix

$I_{V,N}$ at 1 to evaluate $V^*_{I,N}$.

$$\Delta V_C^* = \frac{V_C * (0.9 \times \theta_i^0) - 8 \cdot V_C^*(0.95 \times \theta_i^0) + 8 \cdot V_C^*(1.05 \times \theta_i^0) - V_C^*(1.1 \times \theta_i^0)}{12} \tag{10}$$

Normalized dynamics based Clustering

In our analysis, we perform hierarchical clustering on normalized time-series data for each model variable. For each variable, we calculate the mean (μ_i) and standard deviation (σ_i) of the levels recorded every hour during infection. Variables with zero standard deviation or with a low coefficient of variation ($\frac{\sigma_i}{\mu_i} < 0.05$) were excluded, ensuring retention of only dynamically informative variables. We then normalize the dynamics of the selected variables using Z-score normalisation:

$$z_i(t) = \frac{x_i(t) - \mu_i}{\sigma_i} \tag{11}$$

where $z_i(t)$ denotes the normalised expression of the i-th variable at time t. This normalised matrix was subjected to hierarchical clustering using Ward's linkage method and squared Euclidean distance as the dissimilarity metric:

$$d_{ij} = \sum_{t=1}^{T} \left(z_i(t) - z_j(t)\right)^2 \tag{12}$$

The clustering results were visualised as a heatmap with dendrograms to group variables exhibiting similar temporal dynamics. Subsequently, cluster-wise average expression profiles were plotted over time to capture dominant patterns of activation or suppression.

Quantification of dynamic response under IFN dose variation

To quantify the dynamic differences in variable responses between the two IFN conditions, we use a log-transformed chi-squared–like score computed as follows:

$$\chi_k^2 = \sum_{t=1}^{T} \left[\log_{10}\left(x_k^{(1)}(t)\right) - \log_{10}\left(x_k^{(2)}(t)\right)\right]^2 \tag{13}$$

where ${x_k}^{(1)}(t)$ and ${x_k}^{(2)}(t)$ represent the concentrations of the variable of interest ('x_k') at time t under the two IFN conditions. Condition 1 refers to 100 nM of IFN given 24 hours after an initial IFN dose of 1 nM, whereas Condition 2 refers to 100 nM of IFN given 24 hours after an initial IFN dose of 100 nM. We then rank the variables according to their χ_k^2 values.

Normalized Area over the curve (nAOC) calculation - estimating prophylactic efficiency of IFN pretreatment

To evaluate the prophylactic action, we simulate the effect of various dosages of IFN (as shown in Figure 5) administered k days before the start of infection, where $k \in [0, 1, 2, \ldots 30]$. We report the resulting viral titre at 48 hours post-infection ($V_T(k)$). In the logarithmic scale, we compute the area between this curve ($log_{10}(V_T(t))$) and a horizontal line at $y_{th} = 3$ (a high viral load threshold reference) between $t = 0$ to $t = 30$ days using the trapezoidal rule. Specifically, the AOC was calculated using:

$$AOC = \ nt_{k=0}^{30}(y_{th} - log_{10}(V_T(t))dt \tag{14}$$

Availability of code

Codes for simulation and analysis can be downloaded from our Github repository, `https://github.com/ramyab-986/Integrated_Virus-Immune_Model/tree/master`.

Ethics Statement

This is a computational study. No animals or humans and/or their tissue samples were used.

Author Contributions

Data extraction: RB. Model development, software and formal analysis: RB, HC. Conceptualization, result interpretation and original draft preparation: RB HC RR.

Funding

This work was supported by the Indian Institute of Science Bangalore (RR), Wellcome Trust—DBT India Alliance intermediate fellowship (RR).

Competing interests

The authors declare that they have no competing interests.

References

[1] World Health Organization. WHO coronavirus (covid-19) dashboard: Cases [dashboard]., 2025.

[2] World Health Organization. WHO: Fact sheets: Dengue and severe dengue, 2025.

[3] World Health Organization et al. Global progress report on hiv, viral hepatitis and sexually transmitted infections, 2021: accountability for the global health sector strategies 2016–2021: actions for impact: web annex 1: key data at a glance. In *Global progress report on HIV, viral hepatitis and sexually transmitted infections, 2021: accountability for the global health sector strategies 2016–2021: actions for impact: web annex 1: key data at a glance*. 2021.

[4] World Health Organization. WHO: Fact sheets: Hepatitis C, 2025.

[5] Osamu Takeuchi and Shizuo Akira. Pattern recognition receptors and inflammation. *Cell*, 140(6):805–820, 2010.

[6] Koji Onomoto, Kazuhide Onoguchi, and Mitsutoshi Yoneyama. Regulation of rig-i-like receptor-mediated signaling: interaction between host and viral factors. *Cellular & molecular immunology*, 18(3):539–555, 2021.

[7] William M Schneider, Meike Dittmann Chevillotte, and Charles M Rice. Interferon-stimulated genes: a complex web of host defenses. *Annual review of immunology*, 32(1):513–545, 2014.

[8] John W Schoggins and Charles M Rice. Interferon-stimulated genes and their antiviral effector functions. *Current opinion in virology*, 1(6):519–525, 2011.

[9] Ying Kai Chan and Michaela U Gack. Viral evasion of intracellular dna and rna sensing. *Nature Reviews Microbiology*, 14(6):360–373, 2016.

[10] Dia C Beachboard and Stacy M Horner. Innate immune evasion strategies of dna and rna viruses. *Current opinion in microbiology*, 32:113–119, 2016.

[11] Yunqiang Chen, Yuheng Shi, Jing Wu, and Nan Qi. Mavs: a two-sided card mediating antiviral innate immune signaling and regulating immune homeostasis. *Frontiers in Microbiology*, 12:744348, 2021.

[12] Pranesh Padmanabhan, Urtzi Garaigorta, and Narendra M Dixit. Emergent properties of the interferon-signalling network may underlie the success of hepatitis c treatment. *Nature Communications*, 5(1):3872, 2014.

[13] Katherine Owens, Shadisadat Esmaeili, and Joshua T Schiffer. Heterogeneous sars-cov-2 kinetics due to variable timing and intensity of immune responses. *JCI insight*, 9(9):e176286, 2024.

[14] Lia Van der Hoek. Human coronaviruses: what do they cause? *Antiviral therapy*, 12(4_part_2):651–658, 2007.

[15] Douglas Jie Wen Tay, Zhe Zhang Ryan Lew, Justin Jang Hann Chu, and Kai Sen Tan. Uncovering novel viral innate immune evasion strategies: what has sars-cov-2 taught us? *Frontiers in Microbiology*, 13:844447, 2022.

[16] Marco Binder, Nurgazy Sulaimanov, Diana Clausznitzer, Manuel Schulze, Christian M Hüber, Simon M Lenz, Johannes P Schlöder, Martin Trippler, Ralf Bartenschlager, Volker Lohmann, et al. Replication vesicles are load-and choke-points in the hepatitis c virus lifecycle. *PLoS pathogens*, 9(8):e1003561, 2013.

[17] H. Dahari, R. M. Ribeiro, C. M. Rice, and A. S. Perelson. Mathematical Modeling of Subgenomic Hepatitis C Virus Replication in Huh-7 Cells. *J. Virol.*, 81(2):750–760, Jan 2007.

[18] T. R. Aunins, K. A. Marsh, G. Subramanya, S. L. Uprichard, A. S. Perelson, and A. Chatterjee. Intracellular Hepatitis C Virus Modeling Predicts Infection Dynamics and Viral Protein Mechanisms. *J. Virol.*, 92(11), 06 2018.

[19] Harsh Chhajer, Vaseef A Rizvi, and Rahul Roy. Life cycle process dependencies of positive-sense RNA viruses suggest strategies for inhibiting productive cellular infection. *J R Soc Interface*, 2021.

[20] Carolin Zitzmann, Christopher Dächert, Bianca Schmid, Hilde Van der Schaar, Martijn van Hemert, Alan S Perelson, Frank JM van Kuppeveld, Ralf Bartenschlager, Marco Binder, and Lars Kaderali. Mathematical modeling of plus-strand rna virus replication to identify broad-spectrum antiviral treatment strategies. *PLoS computational biology*, 19(4):e1010423, 2023.

[21] Jaroslaw Smieja, Mohammad Jamaluddin, Allan R Brasier, and Marek Kimmel. Model-based analysis of interferon-β induced signaling pathway. *Bioinformatics*, 24(20):2363–2369, 2008.

[22] Tim Maiwald, Annette Schneider, Hauke Busch, Sven Sahle, Norbert Gretz, Thomas S Weiss, Ursula Kummer, and Ursula Klingmüller. Combining theoretical analysis and experimental data generation reveals irf9 as a crucial factor for accelerating interferon α-induced early antiviral signalling. *The FEBS journal*, 277(22):4741–4754, 2010.

[23] Liang Qiao, Hannah Phipps-Yonas, Boris Hartmann, Thomas M Moran, Stuart C Sealfon, and Fernand Hayot. Immune response modeling of interferon β-pretreated influenza virus-infected human dendritic cells. *Biophysical journal*, 98(4):505–514, 2010.

[24] Frédérique Kok, Marcus Rosenblatt, Melissa Teusel, Tamar Nizharadze, Vladimir Gonçalves Magalhães, Christopher Dächert, Tim Maiwald, Artyom Vlasov, Marvin Wäsch, Silvana Tyufekchieva, et al. Disentangling molecular mechanisms regulating sensitization of interferon alpha signal transduction. *Molecular systems biology*, 16(7):e8955, 2020.

[25] Eirini Kalliara, Malgorzata Kardynska, James Bagnall, David G Spiller, Werner Müller, Dominik Ruckerl, Jarosław Śmieja, Subhra K Biswas, and Pawel Paszek. Post-transcriptional regulatory feedback encodes jak-stat signal memory of interferon stimulation. *Frontiers in Immunology*, 13:947213, 2022.

[26] Jinying Tan, Ruangang Pan, Lei Qiao, Xiufen Zou, and Zishu Pan. Modeling and dynamical analysis of virus-triggered innate immune signaling pathways. *PLoS One*, 7(10):e48114, 2012.

[27] Ulfert Rand, Melanie Rinas, Johannes Schwerk, Gesa Nöhren, Melanie Linnes, Andrea Kröger, Michael Flossdorf, Kristóf Kály-Kullai, Hansjörg Hauser, Thomas Höfer, et al. Multi-layered stochasticity and paracrine signal propagation shape the type-i interferon response. *Molecular systems biology*, 8(1):584, 2012.

[28] Wei Zhang and Xiufen Zou. Systematic analysis of the mechanisms of virus-triggered type i ifn signaling pathways through mathematical modeling. *IEEE/ACM Transactions on Computational Biology and Bioinformatics*, 10(3):771–779, 2013.

[29] Wei Zhang, Tianhai Tian, and Xiufen Zou. Negative feedback contributes to the stochastic expression of the interferon-β gene in virus-triggered type i interferon signaling pathways. *Mathematical biosciences*, 265:12–27, 2015.

[30] Carolin Zitzmann, Bianca Schmid, Alessia Ruggieri, Alan S Perelson, Marco Binder, Ralf Bartenschlager, and Lars Kaderali. A coupled mathematical model of the intracellular replication of dengue virus and the host cell immune response to infection. *Frontiers in microbiology*, 11:725, 2020.

[31] Mauricio Castaño-Arcila, Luis U Aguilera, and Jesus Rodriguez-Gonzalez. Modeling the intracellular dynamics of the dengue viral infection and the innate immune response. *Journal of Theoretical Biology*, 509:110529, 2021.

[32] Michael G Katze, Jamie L Fornek, Robert E Palermo, Kathie-Anne Walters, and Marcus J Korth. Innate immune modulation by rna viruses: emerging insights from functional genomics. *Nature Reviews Immunology*, 8(8):644–654, 2008.

[33] Philipp Hubel, Christian Urban, Valter Bergant, William M Schneider, Barbara Knauer, Alexey Stukalov, Pietro Scaturro, Angelika Mann, Linda Brunotte, Heinrich H Hoffmann, et al. A protein-interaction network of interferon-stimulated genes extends the innate immune system landscape. *Nature immunology*, 20(4):493–502, 2019.

[34] Asmaa Elzawahry, Ashwini Patil, Yutaro Kumagai, Yutaka Suzuki, and Kenta Nakai. Innate immunity interactome dynamics. *Gene Regulation and Systems Biology*, 8:GRSB–S12850, 2014.

[35] Yufan Huang, Huaiyu Dai, and Ruian Ke. Principles of effective and robust innate immune response to viral infections: a multiplex network analysis. *Frontiers in immunology*, 10:1736, 2019.

[36] Sandy S Burkart, Darius Schweinoch, Jamie Frankish, Carola Sparn, Sandra Wüst, Christian Urban, Marta Merlo, Vladimir G Magalhães, Antonio Piras, Andreas Pichlmair, et al. High-resolution kinetic characterization of the rig-i-signaling pathway and the antiviral response. *Life Science Alliance*, 6(10), 2023.

[37] Leo Uchida, Lyre Anni Espada-Murao, Yuki Takamatsu, Kenta Okamoto, Daisuke Hayasaka, Fuxun Yu, Takeshi Nabeshima, Corazon C Buerano, and Kouichi Morita. The dengue virus conceals double-stranded rna in the intracellular membrane to escape from an interferon response. *Scientific reports*, 4(1):7395, 2014.

[38] Akihiko Yoshimura, Tetsuji Naka, and Masato Kubo. Socs proteins, cytokine signalling and immune regulation. *Nature Reviews Immunology*, 7(6):454–465, 2007.

[39] Véronique François-Newton, Gabriel Magno de Freitas Almeida, Béatrice Payelle-Brogard, Danièle Monneron, Lydiane Pichard-Garcia, Jacob Piehler, Sandra Pellegrini, and Gilles Uzé. Usp18-based negative feedback control is induced by type i and type iii interferons and specifically inactivates interferon α response. *PloS one*, 6(7):e22200, 2011.

[40] Jennifer E Fenner, Robyn Starr, Ann L Cornish, Jian-Guo Zhang, Donald Metcalf, Robert D Schreiber, Kathleen Sheehan, Douglas J Hilton, Warren S Alexander, and Paul J Hertzog. Suppressor of cytokine signaling 1 regulates the immune response to infection by a unique inhibition of type i interferon activity. *Nature immunology*, 7(1):33–39, 2006.

[41] Sanne Boersma, Huib H Rabouw, Lucas JM Bruurs, Tonja Pavlovič, Arno LW van Vliet, Joep Beumer, Hans Clevers, Frank JM van Kuppeveld, and Marvin E Tanenbaum. Translation and replication dynamics of single rna viruses. *Cell*, 183(7):1930–1945, 2020.

[42] Da-Yuan Chen, Nazimuddin Khan, Brianna J Close, Raghuveera K Goel, Benjamin Blum, Alexander H Tavares, Devin Kenney, Hasahn L Conway, Jourdan K Ewoldt, Vipul C Chitalia, et al. Sars-cov-2 disrupts proximal elements in the jak-stat pathway. *Journal of virology*, 95(19):10–1128, 2021.

[43] Soheil Rastgou Talemi, Marie Bartenschlager, Bianca Schmid, Alessia Ruggieri, Ralf Bartenschlager, and Thomas Höfer. Dengue virus is sensitive to inhibition prior to productive replication. *Cell Reports*, 37(2), 2021.

[44] Xiufen Zou, Xueshuang Xiang, Yan Chen, Tao Peng, Xuelian Luo, and Zishu Pan. Understanding inhibition of viral proteins on type i ifn signaling pathways with modeling and optimization. *Journal of theoretical biology*, 265(4):691–703, 2010.

[45] Fabio Zanini, Szu-Yuan Pu, Elena Bekerman, Shirit Einav, and Stephen R Quake. Single-cell transcriptional dynamics of flavivirus infection. *Elife*, 7:e32942, 2018.

[46] Justin T O'Neal, Amit A Upadhyay, Amber Wolabaugh, Nirav B Patel, Steven E Bosinger, and Mehul S Suthar. West nile virus-inclusive single-cell rna sequencing reveals heterogeneity in the type i interferon response within single cells. *Journal of virology*, 93(6):10–1128, 2019.

[47] Laura C Van Eyndhoven, Abhyudai Singh, and Jurjen Tel. Decoding the dynamics of multilayered stochastic antiviral ifn-i responses. *Trends in immunology*, 42(9):824–839, 2021.

[48] Mingwei Zhao, Jiangwen Zhang, Hemali Phatnani, Stefanie Scheu, and Tom Maniatis. Stochastic expression of the interferon-β gene. *PLoS biology*, 10(1):e1001249, 2012.

[49] Laura Velazquez, Marc Fellous, George R Stark, and Sandra Pellegrini. A protein tyrosine kinase in the interferon $\alpha\beta$ signaling pathway. *Cell*, 70(2):313–322, 1992.

[50] Michaela Prchal-Murphy, Christian Semper, Caroline Lassnig, Barbara Wallner, Christian Gausterer, Ingeborg Teppner-Klymiuk, Julianna Kobolak, Simone Müller, Thomas Kolbe, Marina Karaghiosoff, et al. Tyk2 kinase activity is required for functional type i interferon responses in vivo. *PloS one*, 7(6):e39141, 2012.

[51] Yoshiyuki Minegishi, Masako Saito, Tomohiro Morio, Ken Watanabe, Kazunaga Agematsu, Shigeru Tsuchiya, Hidetoshi Takada, Toshiro Hara, Nobuaki Kawamura, Tadashi Ariga, et al. Human tyrosine kinase 2 deficiency reveals its requisite roles in multiple cytokine signals involved in innate and acquired immunity. *Immunity*, 25(5):745–755, 2006.

[52] Lionel B Ivashkiv and Laura T Donlin. Regulation of type i interferon responses. *Nature Reviews Immunology*, 14(1):36–49, 2014.

[53] Lisa Miorin, Ana M Maestre, Ana Fernandez-Sesma, and Adolfo García-Sastre. Antagonism of type i interferon by flaviviruses. *Biochemical and biophysical research communications*, 492(4):587–596, 2017.

[54] Antonio Gonçalves, Julie Bertrand, Ruian Ke, Emmanuelle Comets, Xavier De Lamballerie, Denis Malvy, Andrés Pizzorno, Olivier Terrier, Manuel Rosa Calatrava, France Mentré, et al. Timing of antiviral treatment initiation is critical to reduce sars-cov-2 viral load. *CPT: pharmacometrics & systems pharmacology*, 9(9):509–514, 2020.

[55] Jan Rehwinkel and Michaela U Gack. Rig-i-like receptors: their regulation and roles in rna sensing. *Nature Reviews Immunology*, 20(9):537–551, 2020.

[56] Taro Kawai and Shizuo Akira. The role of pattern-recognition receptors in innate immunity: update on toll-like receptors. *Nature immunology*, 11(5):373–384, 2010.

[57] Mitsuharu Sato, Hirofumi Suemori, Naoki Hata, Masataka Asagiri, Kouetsu Ogasawara, Kazuki Nakao, Takeo Nakaya, Motoya Katsuki, Shigeru Noguchi, Nobuyuki Tanaka, et al. Distinct and essential roles of transcription factors irf-3 and irf-7 in response to viruses for ifn-α/β gene induction. *Immunity*, 13(4):539–548, 2000.

[58] Kenya Honda, Akinori Takaoka, and Tadatsugu Taniguchi. Type i inteferon gene induction by the interferon regulatory factor family of transcription factors. *Immunity*, 25(3):349–360, 2006.

[59] Xiao-Dong Li, Lijun Sun, Rashu B Seth, Gabriel Pineda, and Zhijian J Chen. Hepatitis C virus protease ns3/4a cleaves mitochondrial antiviral signaling protein off the mitochondria to evade innate immunity. *Proceedings of the National Academy of Sciences*, 102(49):17717–17722, 2005.

[60] Rak-Kyun Seong, Jae Kyung Lee, and Ok Sarah Shin. Zika virus-induction of the suppressor of cytokine signaling 1/3 contributes to the modulation of viral replication. *Pathogens*, 9(3):163, 2020.

[61] Ren-Jye Lin, Ching-Len Liao, Elong Lin, and Yi-Ling Lin. Blocking of the alpha interferon-induced jak-stat signaling pathway by japanese encephalitis virus infection. *Journal of Virology*, 78(17):9285–9294, 2004.